



Cite this: *Chem. Commun.*, 2025, 61, 2516

Received 3rd November 2024,  
 Accepted 30th December 2024

DOI: 10.1039/d4cc05801a

rsc.li/chemcomm

## Exploration of potential-limited protocols to prevent inefficiencies in Li–O<sub>2</sub> batteries during charge†

Zoé Lacour,<sup>‡ab</sup> Youngjin Ham,<sup>ib ad</sup> Laurence Brazel,<sup>ib a</sup> Clare P. Grey<sup>ib \*ab</sup> and Israel Temprano<sup>ib \*abc</sup>

**Metal–air batteries are promising energy storage systems with high specific energy density and low dependence on critical materials. However, their development is hindered by slow kinetics, low roundtrip efficiency, deficient capacity recovery, and limited lifetime. This work explores the effect of cycling protocols on the lifetime of Li–O<sub>2</sub> cells, and the interplay between electrolyte composition and the upper cut-off voltage during charge. Our results suggest that constant-current-constant-voltage (CCCV) protocols accommodate the slower kinetics at the end of charge in Li–O<sub>2</sub> cells better than the constant-current (CC) protocols majorly used in the field. These results suggest that CCCV protocols should be standardised to assess performance improvements in Li–O<sub>2</sub> cells.**

Diversification of energy storage strategies is an increasingly recognised way to accelerate the energy transition, lowering costs and increasing capacity by reducing the burden on critical materials.<sup>1</sup> From that perspective, secondary Li–air batteries (LABs) offer an interesting alternative to lithium-ion batteries (LIBs) as they rely solely on lithium and carbonaceous materials for their electrode construction, in contrast with the LIBs heavy reliance on transition metals such as cobalt, nickel, manganese, *etc.*<sup>2</sup>

The headline-grabbing high theoretical specific energy of LABs ( $\sim 3500 \text{ W h kg}^{-1}$ ) compared to LIBs ( $\sim 800 \text{ W h kg}^{-1}$ ), is often cited in support of their potential use in applications where energy density is the primary priority, such as transport.<sup>3,4</sup> However, slow kinetics in both the discharge and charge processes, as well as gas filtration/purification requirements, may prove challenging to overcome for the deployment of LABs in electric vehicles.<sup>5</sup> The use of LABs in

stationary battery systems to support decentralised renewable energy generation may, however, be a more suitable application given the lower demands on charging rates and energy density at the system level of this sector. The expected growth in demand for residential and industrial decentralised power generation will add an enormous pressure to global battery production, and therefore to many critical materials, even if EV batteries are widely used in their second-life. The widespread use of LABs as small-scale energy storage can therefore alleviate the huge demand for LIBs and their associated critical resources.<sup>6</sup>

The development of LABs is still, however, at a low technology readiness level (TRL), with multiple fundamental challenges needing to be overcome for their commercialisation.<sup>7</sup> LABs store energy *via* a conversion (rather than intercalation) chemistry, with oxygen as the active cathodic material.<sup>8</sup> During discharge, electrons generated by the oxidation of lithium metal at the anode reach the air electrode, where oxygen is reduced and combined with Li-ions to form insoluble products through the oxygen reduction reaction (ORR).<sup>9</sup> During the charging process, these insoluble discharge products are broken down, with reduced oxygen species being oxidised to O<sub>2</sub> through the oxygen evolution reaction (OER).<sup>10</sup>

The kinetics of the OER are strongly dependent on factors such as the nature, abundance and morphology of discharge products, as well as the mean electron transfer path.<sup>11,12</sup> Therefore, it is expected that these kinetics slow down towards the end of the charging process, as discharge product becomes scarce and the electron transfer path lengthens.<sup>13</sup> This is typically experimentally observed as an increase in overpotential at the end of galvanostatic (constant current, CC) charging of Li–O<sub>2</sub> cells (schematically represented in Fig. 1a).<sup>4</sup>

Although the theoretical LAB cell potential is high, the reaction kinetics are slow, requiring the application of large overpotentials to achieve sufficiently fast charge rates.<sup>14,15</sup> However, these conditions promote undesirable parasitic reactions which rapidly degrade the battery components.<sup>16,17</sup> The decomposition of the discharge products and oxidation of reduced oxygen species at the air electrode is a multifaceted process influenced by the properties of the electrode

<sup>a</sup> Yusuf Hamied Department of Chemistry, University of Cambridge, Cambridge CB21EW, UK

<sup>b</sup> The Faraday Institution, Didcot OX110RA, UK

<sup>c</sup> CICA - Interdisciplinary Center for Chemistry and Biology, University of A Coruña, 15071, A Coruña, Spain. E-mail: i.temprano@udc.es

<sup>d</sup> Cambridge Graphene Centre, University of Cambridge, Cambridge CB30FA, UK

† Electronic supplementary information (ESI) available. See DOI: <https://doi.org/10.1039/d4cc05801a>

‡ Current address: Department of Chemistry, University of Oxford, Oxford OX13TA, UK.





**Fig. 1** Constant current protocol. (a) Typical galvanostatic cycling (CC) potential curves of Li–O<sub>2</sub> cells. (b)–(d) CC potential curves of Li–O<sub>2</sub> cells cycled at a range of upper-cut-off voltages (UCVs); (b) 3.5 V, (c) 3.8 V, and (d) 4.0 V. (e) Discharge and charge capacity per cycle comparison. (f) XRD patterns of electrodes taken after the 10th discharge–charge cycles.

(physical, chemical, and morphological), the electrolyte (viscosity, acceptor number, *etc.*), and the discharge products themselves.<sup>18,19</sup> For instance, slow discharges can produce larger discharge product crystals, which are preferable to the small crystals produced by fast cycles, for high capacity.<sup>20</sup> The latter form thin layers that covers the cathode surface, eventually preventing electron transfer and thus shortening the lifetime.<sup>21</sup>

In this study, we investigate two key and interconnected factors, cycling protocols and electrolyte compositions, both affecting the capacity recovery, overpotentials, and lifetime of Li–O<sub>2</sub> cells. We compare CC and CCCV cycling protocols with a range of upper-cut-off voltages (UCVs) to explore the effect of reducing the current at the end of the charge process, and thus limiting cell overpotentials. The evaluation of these cycling protocols has been performed in cells with and without a redox mediator (RM), which reduces charge overpotentials by catalysing the electron transfer reaction.<sup>22</sup>

A typical plot of voltage *vs* capacity in galvanostatic (constant current, CC) discharge and charge of a Li–O<sub>2</sub> cell is shown in Fig. 1a. The overall reaction at the cathode is  $2\text{Li}^+ + 2\text{e}^- + \text{O}_2 \rightleftharpoons \text{Li}_2\text{O}_2$ , corresponding to a thermodynamic potential of 2.96 V *vs.* Li/Li<sup>+</sup> (dashed line).<sup>23</sup> Even at low rates, the discharge potential is significantly lower than the thermodynamic potential (by  $\sim 0.3$  to 0.5 V) and the charging potential is significantly higher (by  $\sim 0.5$  to 1 V). These deviations, resulting in high voltage hysteresis (overpotential difference between charge and discharge potential curves), indicate significant energy inefficiency. The potential curves of Li–O<sub>2</sub> cells cycled

using a CC protocol typically exhibit 6 regions as shown in Fig. 1a: (i) steep drop in cell potential at the beginning of discharge due to nucleation of the discharge product;<sup>24</sup> (ii) discharge plateau from growth of discharge product;<sup>23</sup> (iii) steep drop in cell potential due to lack of electrode surface and starvation of the ORR;<sup>25</sup> (iv) steep increase in potential at beginning of charge;<sup>26</sup> (v) charge plateau;<sup>18</sup> (vi) steep increase in cell potential at the end of charge due to sluggish kinetics of discharge product decomposition.<sup>9</sup> During step (vi), the faradaic efficiency of the OER reaction drops dramatically (observed in electrochemical mass spectrometry experiments),<sup>17,19,27,28</sup> while parasitic reactions take over.

Li–O<sub>2</sub> cells composed of a lithium metal anode, 1 M LiTFSI in DME electrolyte and a commercial carbon cathode were assembled and cycled using a capacity-limited CC protocol, with upper-cut-off voltages (UCVs) set at 3.5, 3.8, and 4.0 V (Fig. 1b–d). The protocol consisted of a resting period of 8 hours to allow for electrode wetting and oxygen diffusion in the electrolyte, followed by applying a constant current of  $100 \mu\text{A cm}^{-2}$  until the discharge capacity reached  $1 \text{ mA h cm}^{-2}$ , or until the potential dropped below 2 V. Subsequently, the same constant current was applied until the charge capacity reached  $1 \text{ mA h cm}^{-2}$ , or the UCV was reached. The discharge–charge potential curves of these cells over 10 cycles show a steep increase in potential at the beginning of charge, but in all cases the UCV was reached before a charge plateau, and consequently high capacity recovery, could not be achieved (Fig. 1b–d). Fig. 1e shows that, while the discharge capacity limit was reached for most cycles of all cells, very little capacity was recovered upon charge. All cells showed a general increase in charge capacity with cycle number followed by a decrease after cycle 8 for cells with UCV 3.5 V and 3.8 V. The continuous accumulation of discharge product in the air-electrode, as demonstrated by the low charge capacity, is the most likely explanation for this small increase in charging capacity with increasing cycle number.

Postmortem X-ray diffraction (XRD) was performed on the electrodes after the 10 discharge–charge cycles (Fig. 1f). All electrodes cycled using the CC protocol show evidence of residual Li<sub>2</sub>O<sub>2</sub>, with toroidal crystals, typical for Li<sub>2</sub>O<sub>2</sub>,<sup>29</sup> seen in scanning electron microscopy (SEM) images (Fig. S1a–c, ESI†). The cells with UCV 3.5 V and 3.8 V show additional peaks corresponding to LiOH,<sup>30</sup> (Fig. 1f) likely formed through electrolyte decomposition. The absence of LiOH peaks in the XRD pattern of the cell cycled at UCV 4.0 V suggests that this byproduct can be decomposed with sufficient charging time at these potentials. This electrolyte decomposition highlights the need for maintaining low overpotentials in order to extend battery lifetime. The poor capacity recovery observed also indicates the need for rethinking the cycling protocols typically used in the field, which should prioritise energy efficiency whilst maintaining the UCV to a range in which parasitic reactions are minimised.

Li–O<sub>2</sub> cells, assembled in the same way, were then cycled using a capacity-limited CCCV protocol with UCVs also set at 3.5, 3.8 and 4.0 V. The CCCV protocol was identical to the CC protocol during discharge, but after reaching the UCV during charge the voltage was held at this value until the charge capacity reached  $1 \text{ mA h cm}^{-2}$ , or until the current dropped below 10% of its initial value. This potential hold appears as a charge plateau, seen in the discharge–charge potential curves of these cells over 10 cycles



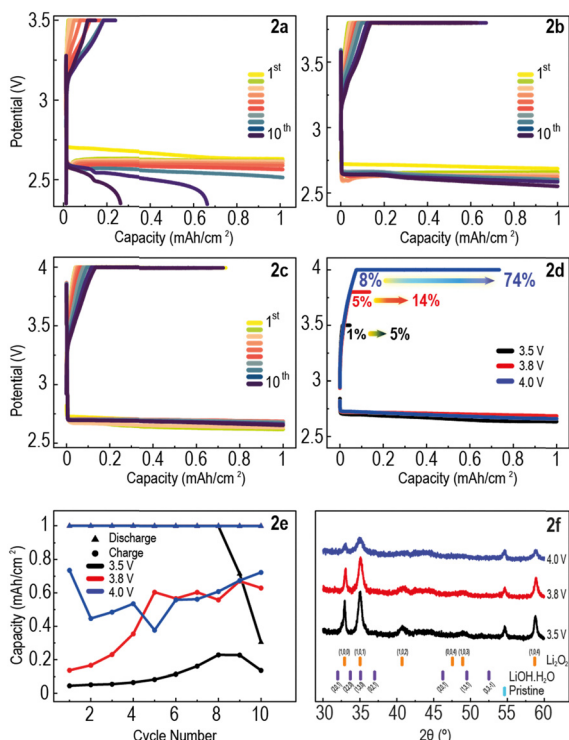


**Fig. 2** Constant current constant voltage protocol. (a)–(c) CCCV potential curves of Li–O<sub>2</sub> cells cycled at a range of upper-cut-off voltages (UCVs); (a) 3.5 V, (b) 3.8 V and (c) 4.0 V. (d) CCCV potential curves of the first discharge–charge cycle of Li–O<sub>2</sub> cells showing capacity recovered during the CC portion of charge and subsequent capacity recovered during the CV portion of charge. (e) Discharge and charge capacity per cycle comparison. (f) XRD patterns of electrodes taken after the 10th discharge–charge cycles.

(Fig. 2a–c). A higher UCV enables both longer constant current (CC) and constant voltage (CV) phases during charging. The former accelerates capacity recovery, as the total current during the CC phase is higher, and the latter increases the capacity recovered before the lower current limit is reached. This is illustrated in Fig. 2d, which shows the first discharge–charge cycle for each cell. As the UCV increases from 3.5 V to 4.0 V, the capacity recovered in the CC phase increases from 1% to 8%, and the total capacity recovered increases from 5% to 74%.

Fig. 2e, similarly to Fig. 1e, shows a general increase in charge capacity with cycle number for all cells, which again is likely attributed to the continuous accumulation of discharge product in the air-electrode, especially in the low UCV cells. An improvement over the CC protocol is evident, particularly for the cells at UCVs 3.8 V and 4.0 V, which demonstrate increases in capacity recovery (CR) for the 10th cycle from 51 to 63% and 34 to 72%, respectively. Fig. 2e also shows this trend, where cells with a higher UCV exhibited greater capacity recovery in most cycles.

Postmortem XRD was performed on the electrodes after the 10 discharge–charge cycles (Fig. 2f). There is no evidence of LiOH, suggesting that any byproduct initially generated by electrolyte decomposition was then fully decomposed due to the increased charging times compared to the CC protocol. The intensity of Li<sub>2</sub>O<sub>2</sub> peaks is significantly lower in the cell cycled with UCV 4.0 V, which corresponds to the higher charge capacity seen in Fig. 2e, confirming

the removal of more Li<sub>2</sub>O<sub>2</sub> from this electrode. This is also observed in the SEM images (Fig. S2a–c, ESI<sup>†</sup>), where significantly less Li<sub>2</sub>O<sub>2</sub> can be seen on the surface of the UCV 4.0 V electrode. These results indicate that CCCV protocols, with reduced currents at the end of charge to accommodate slower OER kinetics,<sup>31–33</sup> enable notably higher CR upon charging than CC protocols, albeit by extending charging times considerably (Fig. S4, ESI<sup>†</sup>).

Subsequently, we studied the use of the redox mediator LiI in conjunction with CCCV protocols. LiI is oxidised to I<sub>3</sub><sup>−</sup> at the positive electrode, I<sub>3</sub><sup>−</sup> then oxidising the Li<sub>2</sub>O<sub>2</sub> and evolving O<sub>2</sub> gas,<sup>22</sup> reducing charge overpotential and increasing capacity recovery.<sup>34–36</sup> Li–O<sub>2</sub> cells with 1 M LiTFSI and 0.1 M LiI in DME were assembled and cycled using the same capacity-limited CCCV protocol with UCVs set at 3.4, 3.5 and 3.8 V. Lower UCVs than in cells without LiI were investigated, to limit the oxidation of I<sup>−</sup> to I<sub>2</sub> above 3.55 V, a highly reactive species that degrades battery components and in turn shortens battery lifetime. The discharge–charge potential curves of these cells (Fig. 3a–c) display a lower charge overpotential than the analogous cells without LiI, and both cells with UCV 3.5 V and 3.8 V show 100% CR upon charge for all 10 cycles (Fig. 3d). A sharp decrease in charge capacity with cycle number for the UCV 3.4 V cell shows that the UCV is too low and therefore reached too quickly to allow full charging on each cycle. Conversely, despite achieving 100% CR in each cycle, the UCV 3.8 V cell forms the degrading I<sub>2</sub> species, which occurs at the third plateau of its charge profile, above 3.55 V.<sup>17,37</sup> Therefore, the cell with UCV 3.5 V is the best-performing in terms of CR at potentials at which OER-competing processes are not likely to happen. The first plateau in this cell's charge profile corresponds to the oxidation of I<sup>−</sup> to I<sub>3</sub><sup>−</sup>, which subsequently oxidises Li<sub>2</sub>O<sub>2</sub> to Li metal and O<sub>2</sub> gas, shown by the second plateau (Fig. 3b).

Postmortem XRD was performed on the electrodes after the 10 discharge–charge cycles (Fig. 3e). The cells with UCV 3.4 V and 3.5 V show low intensity peaks, whereas there is a total absence of peaks in the XRD pattern of the cell cycled at UCV 3.8 V. This correlates well with the high charge capacity seen in Fig. 3d for UCV 3.5 V and 3.8 V, suggesting the discharge product was mostly decomposed upon charging, even without reaching the potentiostatic stage of the CCCV protocol. This is also observed in the SEM images of these electrodes (Fig. S3a–c, ESI<sup>†</sup>), where some film-like Li<sub>2</sub>O<sub>2</sub> can be seen in the UCV 3.4 V cell, whereas in the UCV 3.5 V and 3.8 V cells there is very little to no discharge product visible. This suggests that cycling Li–O<sub>2</sub> cells using a CCCV protocol with a UCV of 3.5 V, combined with a RM, can achieve both higher capacity recovery and longer battery lifetime.

This work illustrates the interplay of cycling protocols and electrolyte composition, and their impact on Li–O<sub>2</sub> cell lifetime. Our results show that allowing for high UCVs to match the discharge capacity in strictly galvanostatic charging results in a shorter lifetime of Li–O<sub>2</sub> cells than adding a potentiostatic stage at the end of charge with lower UCVs. We demonstrate that capacity-limited CCCV charging protocols offer a pronounced improvement over CC protocols in terms of both CR and battery lifetime. While lowering the UCV is key for extending cell lifetime, achieving this without compromising CR remains difficult. Therefore, the challenge of keeping the UCV as low as possible to manage parasitic reactions while still recovering 100% capacity at a reasonable charging rate should be the focus of much more attention in the field.





**Fig. 3** Constant current constant voltage protocol with redox mediator. (a)–(c) CCCV potential curves of Li–O<sub>2</sub> cells containing Lil as a redox mediator in the electrolyte cycled at a range of upper-cut-off voltages (UCVs); (a) 3.4 V, (b) 3.5 V and (c) 3.8 V. (d) Discharge and charge capacity per cycle comparison. (e) XRD patterns of electrodes taken after the 10th discharge–charge cycles.

This work was supported by the Faraday Institution (grant number FITG-FUSE-078). I. T. acknowledges support from a Beatriz Galindo senior fellowship (BG22/00148) from the Spanish Ministry of Science and Innovation. L. B. acknowledges support from the EPSRC through the NanoDTC (grant no. EP/S022953/1), as well as from Cambridge Display Technology Ltd.

## Data availability

Data for this article is available at symplectic elements at <https://elements.admin.cam.ac.uk/viewobject.html?cid=1&id=1656199>.

## Conflicts of interest

There are no conflicts to declare.

## Notes and references

- M. Arbabzadeh, R. Sioshansi, J. X. Johnson and G. A. Keoleian, *Nat. Commun.*, 2019, **10**, 3413.
- C. Grey and J. Tarascon, *Nat. Mater.*, 2017, **16**, 45–56.
- T. Liu, J. P. Vivek, E. W. Zhao, J. Lei, N. Garcia-Araez and C. P. Grey, *Chem. Rev.*, 2020, **120**, 6558–6625.
- Z. Gao, I. Temprano, J. Lei, L. Tang, J. Li, C. P. Grey and T. Liu, *Adv. Mater.*, 2023, **35**, 2201384.
- L. A. Archer, P. G. Bruce, E. J. Calvo, D. Dewar, J. H. J. Ellison, S. A. Freunberger, X. Gao, L. J. Hardwick, G. Horwitz, J. Janek, L. R. Johnson, J. W. Jordan, S. Matsuda, S. Menkin, S. Mondal,

- Q. Qiu, T. Samarakoon, I. Temprano, K. Uosaki, G. Vailaya, E. D. Wachsman, Y. Wu and S. Ye, *Faraday Discuss.*, 2024, **248**, 392.
- W.-J. Kwak, Rosy, D. Sharon, C. Xia, H. Kim, L. R. Johnson, P. G. Bruce, L. F. Nazar, Y.-K. Sun and A. A. Frimer, *Chem. Rev.*, 2020, **120**, 6626–6683.
- G. A. Attard, E. J. Calvo, L. A. Curtiss, D. Dewar, J. H. J. Ellison, X. Gao, C. P. Grey, L. J. Hardwick, G. Horwitz, J. Janek, L. R. Johnson, J. W. Jordan, S. Matsuda, S. Mondal, A. R. Neale, N. Ortiz-Vitoriano, I. Temprano, G. Vailaya, E. D. Wachsman, H.-H. Wang, Y. Wu and S. Ye, *Faraday Discuss.*, 2024, **248**, 75.
- L. Luo, B. Liu, S. Song, W. Xu, J.-G. Zhang and C. Wang, *Nat. Nanotechnol.*, 2017, **12**, 535–539.
- Y.-C. Lu, B. M. Gallant, D. G. Kwabi, J. R. Harding, R. R. Mitchell, M. S. Whittingham and Y. Shao-Horn, *Energy Environ. Sci.*, 2013, **6**, 750–768.
- H.-D. Lim, B. Lee, Y. Bae, H. Park, Y. Ko, H. Kim, J. Kim and K. Kang, *Chem. Soc. Rev.*, 2017, **46**, 2873–2888.
- L. Liu, Y. Liu, C. Wang, X. Peng, W. Fang, Y. Hou, J. Wang, J. Ye and Y. Wu, *Small Methods*, 2022, **6**, 2101280.
- G. A. Attard, P. G. Bruce, E. J. Calvo, Y. Chen, L. A. Curtiss, D. Dewar, J. H. J. Ellison, J. Fernández-Vidal, S. A. Freunberger, X. Gao, C. P. Grey, L. J. Hardwick, G. Horwitz, J. Janek, L. R. Johnson, E. Jónsson, S. Karunaratne, S. Matsuda, S. Menkin, S. Mondal, S. Nakanishi, N. Ortiz-Vitoriano, Z. Peng, J. P. Rivera, I. Temprano, K. Uosaki, E. D. Wachsman, Y. Wu and S. Ye, *Faraday Discuss.*, 2024, **248**, 210.
- N. B. Aetukuri, B. D. McCloskey, J. M. García, L. E. Krupp, V. Viswanathan and A. C. Luntz, *Nat. Chem.*, 2015, **7**, 50–56.
- R. Gao, X. Liang, P. Yin, J. Wang, Y. L. Lee, Z. Hu and X. Liu, *Nano Energy*, 2017, **41**, 535–542.
- C. Xia, M. Waletzko, L. Chen, K. Peppler and P. J. Klar, and J. R. Janek, *ACS Appl. Mater. Interfaces*, 2014, **6**, 12083–12092.
- P. Zhang, M. Ding, X. Li, C. Li, Z. Li and L. Yin, *Adv. Energy Mater.*, 2020, **10**, 2001789.
- A. Nakanishi, M. L. Thomas, H.-M. Kwon, Y. Kobayashi, R. Tatara, K. Ueno, K. Dokko and M. Watanabe, *J. Phys. Chem. C*, 2018, **122**, 1522–1534.
- L. Johnson, C. Li, Z. Liu, Y. Chen, S. A. Freunberger, P. C. Ashok, B. B. Praveen, K. Dholakia, J.-M. Tarascon and P. G. Bruce, *Nat. Chem.*, 2014, **6**, 1091–1099.
- I. Temprano, T. Liu, E. Petrucco, J. H. Ellison, G. Kim, E. Jónsson and C. P. Grey, *Joule*, 2020, **4**, 2501–2520.
- B. M. Gallant, D. G. Kwabi, R. R. Mitchell, J. Zhou, C. V. Thompson and Y. Shao-Horn, *Energy Environ. Sci.*, 2013, **6**, 2518–2528.
- B. D. Adams, C. Radtke, R. Black, M. L. Trudeau, K. Zaghbib and L. F. Nazar, *Energy Environ. Sci.*, 2013, **6**, 1772–1778.
- J. B. Park, S. H. Lee, H. G. Jung, D. Aurbach and Y. K. Sun, *Adv. Mater.*, 2018, **30**, 1704162.
- Y.-C. Lu, H. A. Gasteiger, M. C. Parent, V. Chiloyan and Y. Shao-Horn, *Electrochem. Solid-State Lett.*, 2010, **13**, A69.
- S. Lau and L. A. Archer, *Nano Lett.*, 2015, **15**, 5995–6002.
- J. Højberg, B. D. McCloskey, J. Hjelm, T. Vegge, K. Johansen, P. Norby and A. C. Luntz, *ACS Appl. Mater. Interfaces*, 2015, **7**, 4039–4047.
- J. Chen, E. Quattrocchi, F. Ciucci and Y. Chen, *Chem*, 2023, **9**, 2267–2281.
- B. D. McCloskey, D. Bethune, R. Shelby, T. Mori, R. Scheffler, A. Speidel, M. Sherwood and A. Luntz, *J. Phys. Chem. Lett.*, 2012, **3**, 3043–3047.
- S. Das, J. Højberg, K. B. Knudsen, R. Younesi, P. Johansson, P. Norby and T. Vegge, *J. Phys. Chem. C*, 2015, **119**, 18084–18090.
- Z. Z. Shen, C. Zhou, R. Wen and L. J. Wan, *Chin. J. Chem.*, 2021, **39**, 2668–2672.
- N. Alcock, *Acta Crystallogr.*, 1971, **27**, 1682–1683.
- Z. Su, I. Temprano, N. Folastre, V. Vanpeene, J. Villanova, G. Gachot, E. V. Shevchenko, C. P. Grey, A. A. Franco and A. Demortière, *Small Methods*, 2024, **8**, 2300452.
- K. Ku, S.-B. Son, J. Gim, J. Park, Y. Liang, A. Stark, E. Lee and J. Libera, *J. Mater. Chem. A*, 2022, **10**, 288–295.
- E. A. Kedzie, J. E. Nichols and B. D. McCloskey, *J. Mater. Res.*, 2022, **37**, 3227–3236.
- H.-D. Lim, B. Lee, Y. Zheng, J. Hong, J. Kim, H. Gwon, Y. Ko, M. Lee, K. Cho and K. Kang, *Nat. Energy*, 2016, **1**, 1–9.
- T. Liu, J. T. Frith, G. Kim, R. N. Kerber, N. Dubouis, Y. Shao, Z. Liu, P. C. Magusin, M. T. Casford and N. Garcia-Araez, *J. Am. Chem. Soc.*, 2018, **140**, 1428–1437.
- E. Jónsson, A. H. Berge, C. P. Grey and I. Temprano, *Faraday Discuss.*, 2024, **248**, 145.
- C. L. Bentley, A. M. Bond, A. F. Hollenkamp, P. J. Mahon and J. Zhang, *J. Phys. Chem. C*, 2015, **119**, 22392–22403.

